Design Process of IDT Aided by Multiphysics FE Analyses

Adam Martowicz, Mateusz Rosiek, Michal Manka, Tadeusz Uhl
AGH University of Science and Technology,
Faculty of Mechanical Engineering and Robotics,
Department of Robotics and Mechatronics,
al. A. Mickiewicza 30, 30-059 Krakow, Poland
adam.martowicz@agh.edu.pl, rosiek@agh.edu.pl, mmanka@agh.edu.pl, tuhl@agh.edu.pl

ABSTRACT
Presented work is devoted to a design process performed for the interdigital transducer, which is a perspective application for the area of structural health monitoring. In order to obtain the desirable characteristic of the transducer fully coupled numerical analyses were performed in ANSYS Multiphysics software. Utilised finite element models considered both structural dynamics and properties of used piezoelectric material. The process of design improvement was preceded by the sensitivity analysis. In order to search for the best electrode pattern selected geometrical features of the transducer were assumed to vary within allowed ranges. The design parameters, which were taken into account, related to the efficiency of proposed transducer design for the emission of acoustic waves in the monitored structure. The search objectives considered the criteria related to the shape of the beampattern and amplitudes of generated Lamb waves. As a result of the optimization procedure, the simultaneous increase of anti-symmetric mode amplitude and the reduction of undesirable symmetric mode amplitude of generated Lamb waves in the direction perpendicular to the transducer fingers was expected. Another aim of the optimization was to minimize the main lobe width and undesirable contribution of both symmetric and anti-symmetric waves in the parallel direction to the transducer fingers. The response surface method and genetic algorithms were used for fast and effective search through the input design domain.

Keywords: interdigital transducer; Lamb waves; structural health monitoring; nondestructive testing; multiphysics; finite element method; sensitivity analysis; design process; response surface method; genetic algorithms.

INTRODUCTION

In modern engineering the measurement-related activities behind the structural health monitoring (SHM) stand for key issues. Their relevance results from the need of long, low-cost and safe operation of monitored mechanical structures. The main reason to build SHM systems is effective identification of the structural damage at its early stage end therefore

prevention from major failure of monitored construction. Amongst all measurement techniques which are known in the area of non-destructive testing, the techniques based on the Lamb waves propagation have recently appeared as promising ones for damage detection [1]. The Lamb waves are type of ultrasonic guided waves which can propagate in thin-walled structures with parallel free boundaries, e.g. plates, shells or pipes. The Lamb waves can travel in different types of materials and over long distances with very little amplitude loss. Hence the monitoring of large areas carried out with the use of relatively small number of sensors is feasible. Moreover, the measurement techniques based on the Lamb waves allow for examination of entire cross-section of the structure and are very sensitive to multiple types of defects [2]. The Lamb waves stand for a superposition of longitudinal and shear modes of ultrasonic waves. The characteristics of generated waves depends on structural geometry and excitation method. The Lamb waves can propagate in both symmetric and anti-symmetric modes as presented in Figure 1.

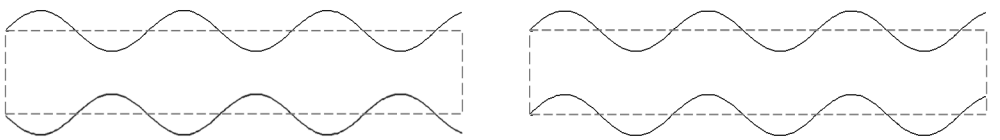

Figure 1. The symmetric (left) and anti-symmetric (right) Lamb wave mode

Both symmetric and antisymmetric modes can be respectively determined with the following formulas [3]:

$$\frac{\tan(q*h)}{\tan(p*h)} = \frac{4k^2qp}{(k^2-q^2)^2} \tag{1}$$

$$\frac{\tan(q*h)}{\tan(p*h)} = \frac{(k^2-q^2)^2}{4k^2qp} \tag{2}$$

where:

$$p^2 = \frac{\omega^2}{c_L^2} - k^2 \tag{3}$$

$$q^2 = \frac{\omega^2}{c_T^2} - k^2 \tag{4}$$

$$k = \frac{\omega}{c_p} \tag{5}$$

h, k, c_L, c_T, c_p, ω are respectively: plate thickness, wave number, velocities of longitudinal and transverse modes, phase velocity and wave circular frequency. The specificity of properties of the Lamb waves allows for effective applications in SHM systems [1,4,5,6]. While propagating through monitored structure the waves get reflected, modulated when they meet flaws. Determined times of flight and frequency characteristics enable for the inference on the structure condition.

Amongst currently used transducers which are applied for the Lamb wave generation and

measurement the most known types are: ultrasonic probes [7,8], electromagnetic acoustic transducers (EMAT) [9], laser systems [10,11], capacitive micromachined ultrasonic transducers (CMUT) [12,13,14,15,16], piezoelectric transducers [17,18], mainly including macro fibre composites (MFC) [19,20,21] as well as interdigital transducers (IDT) [22,23]. Main characteristics of each mentioned measurement technique are briefly discussed below.

Ultrasonic probes are used for generation and measurement of bulk waves however they can also be successfully adopted for the Lamb wave based measurement. This measurement can be achieved by the application of angle-adjustable perspex wedges or buffer rods to achieve Hertzian contact transducer. Described approach characterizes high precision and controllability as well as narrow band wave generation. The disadvantage of the application of ultrasonic probes is however high sensitivity of their effectiveness to the quality of coupling between probe and surface of monitored structure.

EMAT allow for remote generation of the Lamb waves by electromagnetic coupling between meandering coil and monitored electrically conducting structure. The spacing between coil turns coincides with a half of the wavelength. The main advantages of EMAT are contactless measurements, directional generation of the wave with desired polarization. The inconvenience is that only structures made of ferromagnetic materials can be monitored additionally ensuring very small distance to the transducer.

Laser systems stand for other noncontact methods for generating and measuring the Lamb waves. Both broadband or narrowband transducers are used depending on the application area and the frequency range. The most known applications of laser system are the measurements based on the analysis of changes of the light flux characteristics that reaches a photodetector. Other methods are based on the laser interferometry, i.e. with Fabry-Perrot's and Michelson's interferometric detectors. The most convenient method for laser based ultrasound waves generation is the usage of shadow mask. More efficient are measurement methods making use of lenticular lens or diffraction gratings. The latter are however more expensive and harder to implement. Laser based transducers do not require the presence of the couplant and can work for wide variety of frequencies. The disadvantages of applications are low energy of emitted wave and high cost of transducers. Additionally the measurement may be performed only for reflective, flat and smooth surfaces.

CMUT consist of electrostatically actuated micron-size membranes suspended over a silicon substrate. Deposited passivation layer prevents form chemical reactions with surrounding media in case of immersed application. Alternating voltage with DC bias generated in integrated electronic circuit is applied to power electrodes and makes the membrane vibrate. Usually CMUT cells are manufactured as linear arrays or 2D matrices to increase the energy of emitted acoustic wave. Integrated electronic circuit with processor allow for the control of power supply for all cells. CMUT may operate as both generator and receiver of the acoustic waves. The main advantages of CMUT are: acoustic impedance match with surrounding air and liquids, small size, potential integration with on-board electronics, high sensitivity, tunable electromechanical coupling coefficient by changing bias voltage, design flexibility allowing for both 1D and 2D arrays. However the pressure of generated waves is small therefore the energy transferred to mechanical structure may appear as insufficient for effective monitoring. Moreover high bias voltage may lead to collapse of the CMUT membranes.

Piezoelectric transducers are nowadays one of the most commonly applied components used for the Lamb wave generation and measurements resulting from converse and direct piezoelectric effect respectively. Piezoelectric transducers typically stand for either monolayer patches or multilayer stacks made of lead zirconate titanate (PZT). Relatively low

costs of the application of piezoelectric components makes the whole measurement system affordable. Moreover described measurement technique characterizes low power consumption, negligible masses and sizes of piezoelectric transducers, acoustic impedance match with metal and composite structure impedance as well as high energy of generated waves. The disadvantages of the PZT transducers are multiple mode wave generation, the work at high voltage and life cycle limitations. Additionally the temperature constrain on the application area appears. The exceedance of the Curie temperature results in loss of piezoelectric properties.

MFC were proposed to increase flexibility and durability of commonly applied PZT transducers. They are composed with thin unidirectionally aligned PZT fibres covered with two sets of electrode patterns printed on a polymer film, e.g. made of polyimide. MFC allow for both generation and measurement of the Lamb waves along chosen directions. There are known applications of a rosette-type and MFC based sensors used for the direction detection of the approaching wave. The other advantages of MFC transducers are relatively low cost of application, large area coverage in case of a rosette configuration and high energy of generated waves. Some inconvenience may relate to relatively large size of MFC.

The last group of transducers which is discussed is IDT. IDT stand for relatively novel construction in SHM, however the theory behind recent applications of IDT was born in the XIX-th century. Typically IDT are built with the following layers: bottom layer i.e. ground electrode, layer made of piezoelectric material and top layer with top electrodes. Bottom electrode usually covers the whole bottom surface of piezoelectric material. Piezoelectric layer may be made of piezoelectric polymer, e.g. PVDF, piezoelectric ceramic material or piezoelectric composite, e.g. MFC. IDT which are mounted on monitored structure are the most commonly applied electromechanical components for narrow band Lamb waves generation. The main advantages of IDT are selectivity and directivity of generated guided waves which allows for both localization of damage, even of small size, and decrease of electrical energy consumption. The electromechanical coupling factor is however lower than for the standard piezoelectric transducer. Moreover there is limited temperature range for IDT based on PVDF. Residual stresses created during bonding process may significantly reduce the life time.

In the paper a design process for chosen IDT is presented. The work covers the following topics: section 2 presents the structure of IDT and guidelines for pattern design, section 3 describes elaborated FE model of an aluminium plate with mounted IDT, section 4 presents the workflow for carried out dynamic FE analyses with exemplary results, section 5 describes the results of sensitivity analysis, section 6 discusses design configurations obtained with the application of response surface method (RSM) and genetic algorithms (GA), final section 7 summarizes the paper and presents concluding remarks.

2. IDT – STRUCTURE AND PATTERN DESIGN

The structure of IDT is presented in Figure 2. Figure 3 shows an exemplary IDT tested with laboratory setup. As already mentioned in the introductory section, IDT in a typical single comb configuration consists of 3 layers providing both outer layers with electrodes (bottom ground GND, and top V+, V- supplied with sine wave voltage) and piezoelectric material as the inner layer.

Elasticity of the transducer, maximal energy as well as the frequency range of generated waves are determined by used piezoelectric material. The key issue for IDT is however the pattern of the top electrodes. Typically they characterize a comb-type shape of patterns. Distance between the fingers belonging to the same electrode defines the length of generated wave λ.

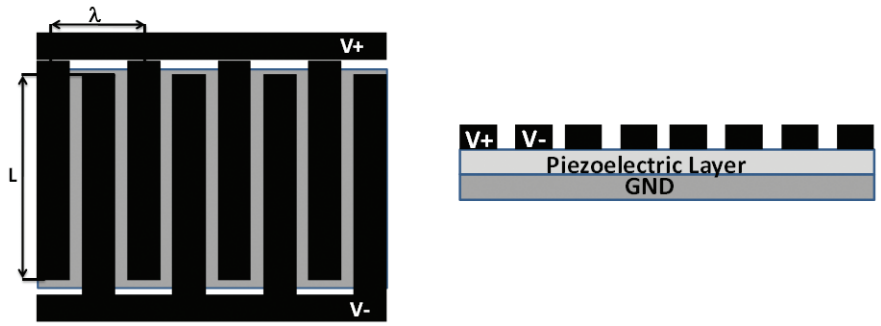

Figure 2. The structure of IDT

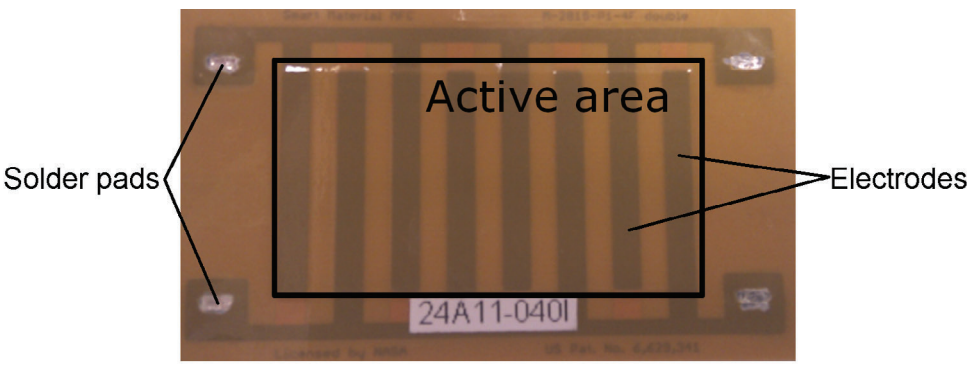

Figure 3. An example of tested IDT

The design process of IDT is based on group and phase velocity dispersion curves that should be determined for chosen material and thickness of monitored plate. Figure 4 and 5 respectively present exemplary group and phase velocity dispersion curves determined for a 4mm-thick aluminium plate.

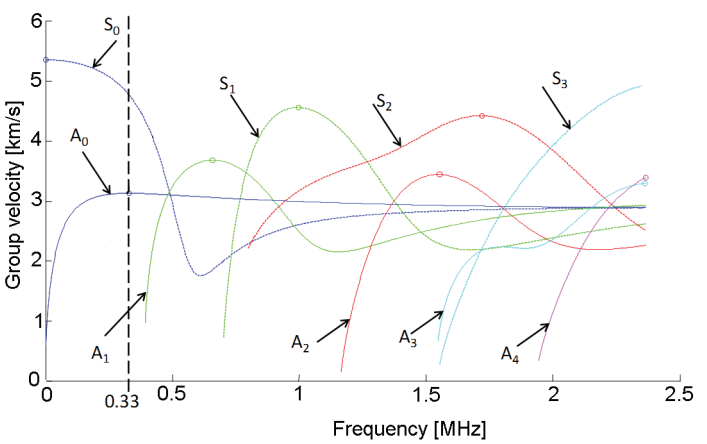

Figure 4. Group velocity dispersion curves for aluminium plate

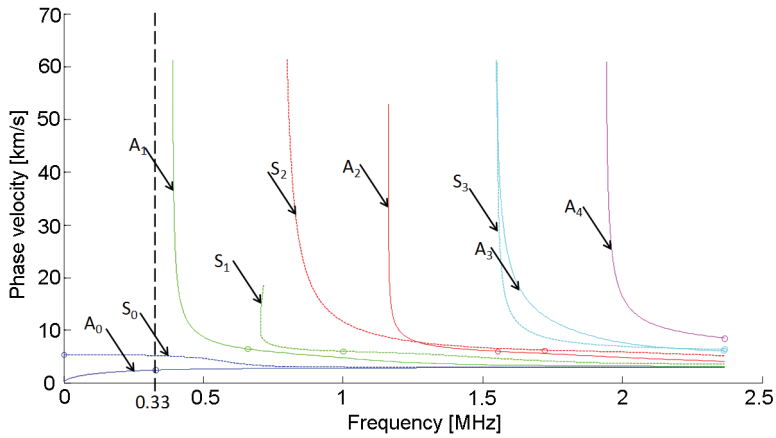

Figure 5. Phase velocity dispersion curves for aluminium plate

For presented case the A0 mode is considered to be generated in aluminium plate. Hence the frequency is determined for which the sensitivity of group velocity related to the A0 mode is the smallest, i.e. for which the dispersion of the A0 mode is the least significant. Found frequency f equals 330kHz. Next the phase velocity c_p is found for the frequency f on the phase velocity dispersion curves (Figure 5). c_p equals 2475m/s. Finally the wave length λ for the A0 mode can be calculated with the following formula:

$$\lambda = \frac{c_p}{f} = 7.5mm \tag{6}$$

The Lamb waves are mostly generated in the direction perpendicular to the electrode fingers. Similarly, IDT with perpendicular orientation of fingers regarding the direction of approaching waves are more sensitive as presented in Figure 6. Shown time history plots were obtained for both perpendicular and parallel orientations of the IDT sensor.

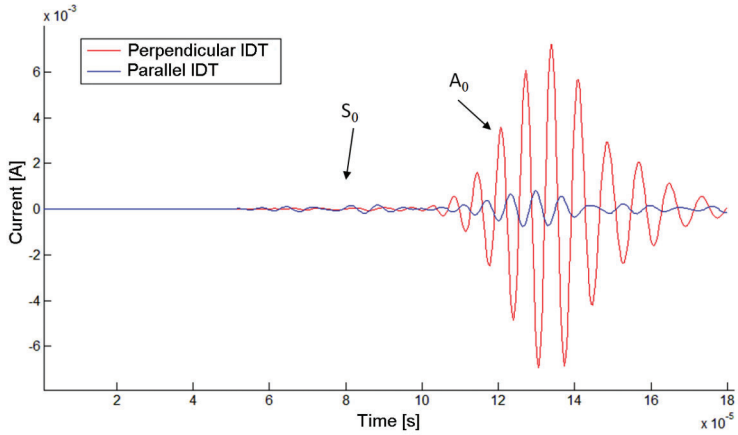

Figure 6. Measured current for different orientations of IDT sensor

Divergence of the Lamb waves is dependent on the fingers length L. The formula used to calculate the beam divergence angle α takes the following form:

$$\alpha = \arcsin(\frac{\lambda}{L}) \tag{7}$$

For presented IDT the length of fingers is 15mm what results in divergence angle 30deg.

Further improvements on the IDT construction may deal with the number of comb electrodes and shapes of fingers. First, a double comb configuration can be considered to increase the amplitude of generated Lamb wave (Figure 7) [24] as well as apodized electrodes pattern for better control of wave directivity (Figure 8) [25,26]. In case of double comb configuration the comb-shaped electrodes are localized on both outer layers of IDT. Additionally for apodized IDT, both the length and width of subsequent fingers vary.

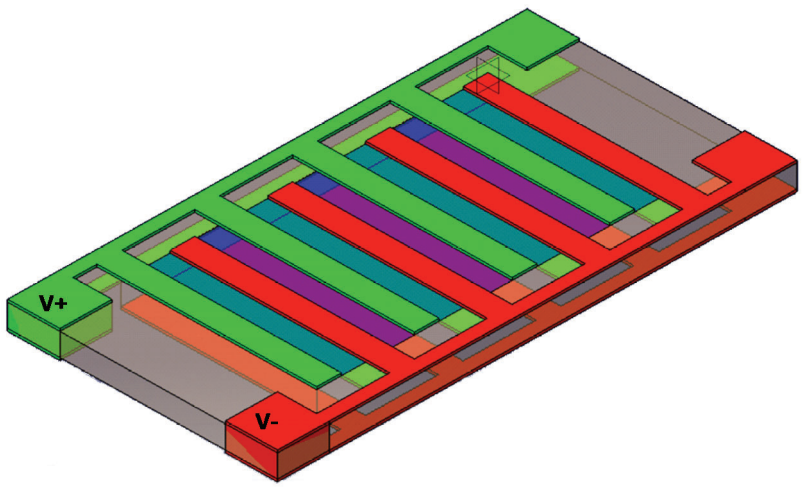

Figure 7. Double comb configuration of IDT

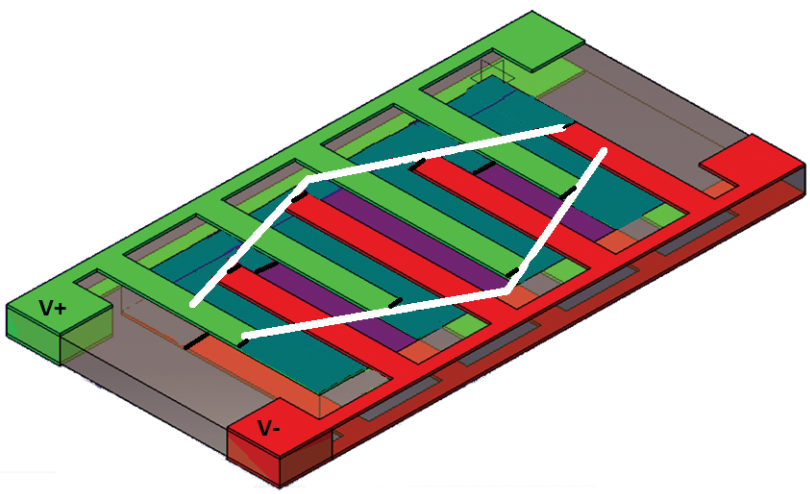

Figure 8. Double comb configuration of IDT with apodized electrodes pattern

In present study there is assumed double comb and apodized configuration of designed IDT. All the details on modelling as well as allowed ranges of design parameters are described in the following section.

3. FE MODEL

Elaborated FE model of a 4mm-thick aluminium plate with mounted IDT, which was used for the simulation of the Lamb wave propagation, is presented in Figure 9. There was modelled double comb apodized IDT as shown in Figure 10. The model was prepared in ANSYS/Multiphysics software using 20-node parabolic brick elements [27].

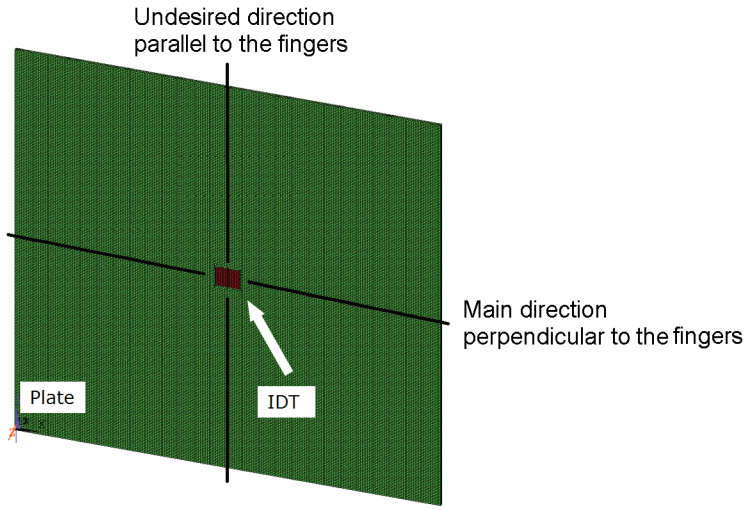

Figure 9. FE model of an aluminium plate with IDT

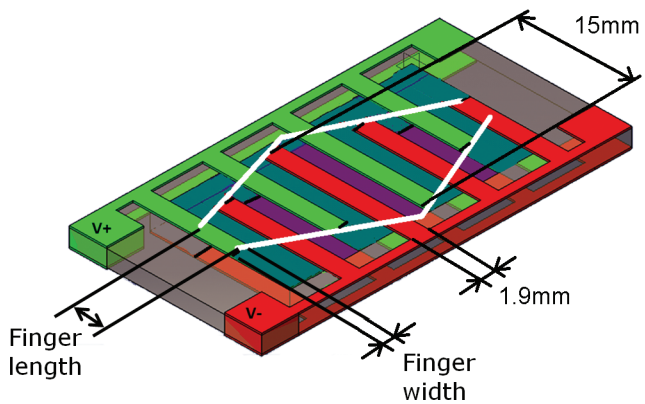

Figure 10. Double comb configuration of IDT with apodized electrodes pattern

The wave length was determined for the case presented in section 2, i.e. $\lambda = 7.5$mm as found for the A0 mode of generated Lamb wave. The maximal value of the finger length equals 15mm. The thickness of piezoelectric layer equals 0.18mm. This layer was modelled

as MFC acting with the configuration of d_{31}-effect. This effect means that the directions related respectively to the maximal strain and the electric field are perpendicular. The properties of piezoelectric material are presented in Table 1. The MFC was modelled as a solid material with approximated characteristics representing the resultant properties of both PZT fibers and polymer [28].

Table 1. Properties of used piezoelectric material

$c^E_{11} = 3.94 * 10^{10}$ Pa	$c^E_{22} = 2.03 * 10^{10}$ Pa	$c^E_{33} = 3.25 * 10^{10}$ Pa
$c^E_{12} = 1.29 * 10^{10}$ Pa	$c^E_{13} = 0.83 * 10^{10}$ Pa	$c^E_{23} = 0.53 * 10^{10}$ Pa
$c^E_{44} = 0.55 * 10^{10}$ Pa	$c^E_{55} = 0.55 * 10^{10}$ Pa	$c^E_{66} = 1.31 \times 10^{10}$ Pa
$e_{31} = -7.12$ C m^{-2}	$e_{33} = 12.1$ C m^{-2}	$e_{32} = -4.53$ C m^{-2}
$e_{24} = -17.03$ C m^{-2}	$e_{15} = -17.03$ C m–2	$\rho = 7000$ kg m^{-3}
$\varepsilon^{\varepsilon}_{11} = 237.2\varepsilon_0$ C V^{-1} m^{-1}	$\varepsilon^{\varepsilon}_{22} = 237.2\varepsilon_0$ C V^{-1} m^{-1}	$\varepsilon^{\varepsilon}_{33} = 143.4\varepsilon_0$ C V^{-1} m^{-1}

Applied apodization assumes a linear decrease of both width and length of subsequent fingers starting with the middle ones which characterize the maximal values of mentioned dimensions, i.e. always 1.9mm and 15mm respectively, as shown in Figure 10. The outer fingers are of the smallest dimensions. For the study there is considered the following variation of the width and length of outer fingers:

- finger width *W*: [0.7mm,1.9mm]
- finger length *L*: [3mm,12mm]

The parameters *W* and *L* are finally defined as the design variables describing selected design configuration to be checked in terms of chosen criteria. They are described in the following sections. In the simulations the amplitude of voltage used to supply both electrodes V+ and V- equals 100V.

4. DYNAMIC FE ANALYSES

Fully-coupled transient analyses were carried out considering both structural dynamics and properties of piezoelectric material. A five-cycle tone burst modulated with Hanning window was applied for the voltage excitation at the frequency 330kHz. Simulated time equals 70μs. Numerical simulations were performed to allow for the sensitivity analysis and for design optimization aided with the RSM [29,30,31]. The approximating techniques allowed for considerable time savings.

For parameterized FE model of the plate with mounted IDT the dynamic analyses were performed accordingly to the workflow presented in Figure 11. 20 design configurations were checked for assumed ranges of variation for the parameters *W* and *L*. Studied design configurations were found as all possible combinations of the following values of the length *W* and the width *L* of outer fingers:

- finger width *W*: {0.7mm, 1mm, 1.3mm, 1.6mm, 1.9mm}
- finger length *L*: {3mm, 6mm, 9mm, 12mm}

Figure 12 shows the out-of-plane nodal displacements for the aluminium plate resulting from the Lamb wave propagation. Larger deformations relate to the desired A0 mode.

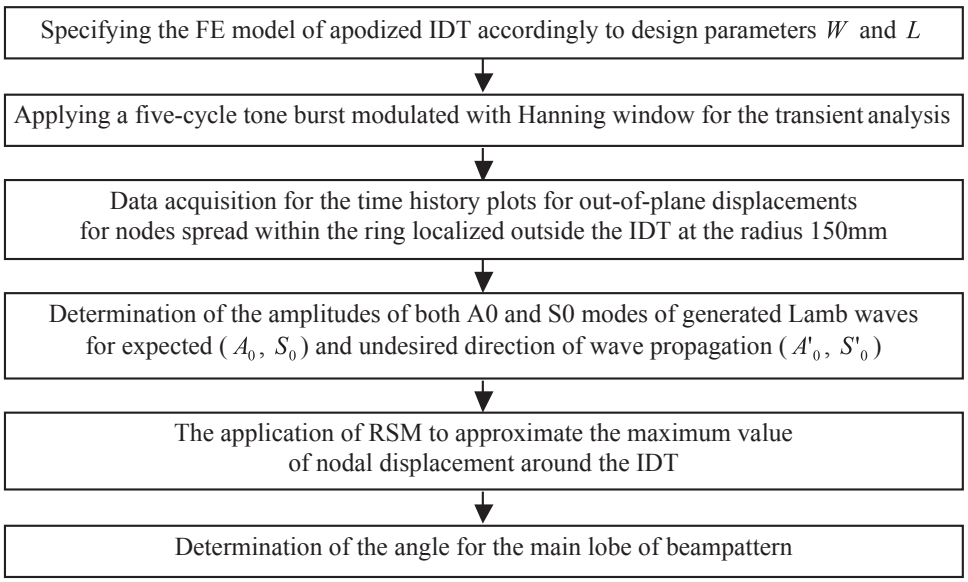

Figure 11. Workflow used for the calculations of characteristics of mounted IDT

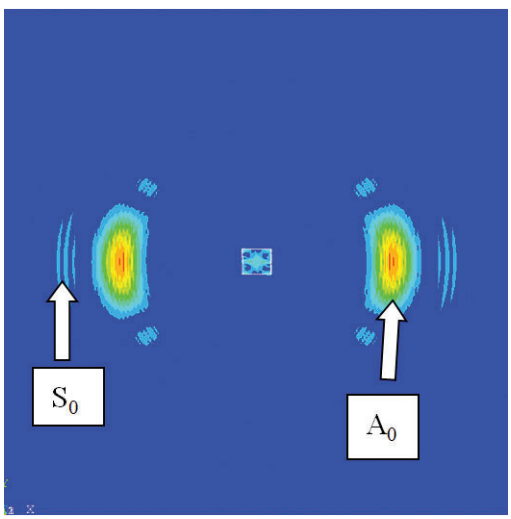

Figure 12. Lamb wave propagation in modelled aluminium plate

Virtual sensors for the out-of-plane deformation measurement are spread within the ring as presented in Figure 13. When the data acquisition process is completed there are found the amplitudes of both A0 and S0 modes of generated Lamb waves for expected direction (horizontal direction in Figure 13), i.e. A_0, S_0 and undesired direction of wave propagation (vertical direction), i.e. A'_0, S'_0. The measurement points for this analysis were localized respectively 150mm to the left and 150mm above the centre of IDT. An example of the time history plot of nodal displacements as well as determined envelope are shown in Figure 14. The first maximum represents the S0 mode which is faster than the A0 mode.

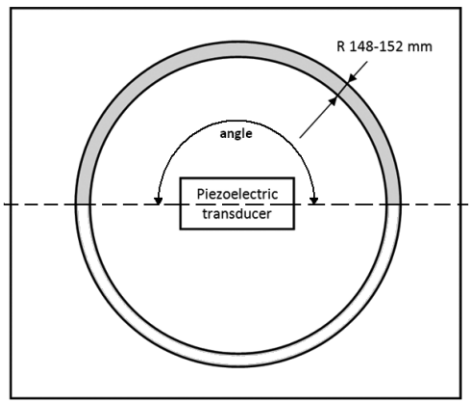

Figure 13. The localization of measurement nodes

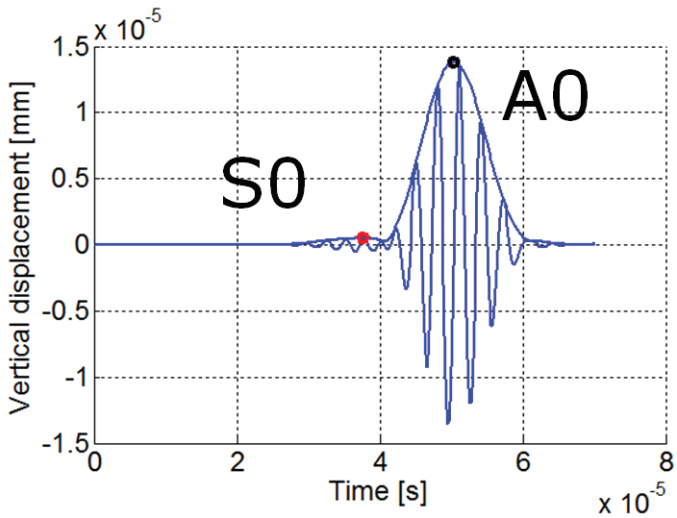

Figure 14. Example of the time history plot of nodal displacements

When the amplitudes A_0, S_0, A'_0 and S'_0 are determined, the RSM is applied to approximate the maximum value of nodal displacement within the area of already defined ring around the IDT. Approximated parameter was defined as the maximal value of the Hilbert transform calculated for the out-of-plane nodal displacement. The metamodeling procedure was performed on the basis of all nodal displacements found for all nodes localized in mentioned area. For the reason of model symmetry only an upper half of the ring was considered. Then all the coordinates of nodes were transformed from originally used Euclidean system to polar system so that a simple shape of design domain could be achieved. By doing so the input domain became of the rectangular shape which was easy to be specified by 2 intervals:

- the angle: [0,πrad]
- the radius: [148mm,152mm]

Finally the normalization of the angle as well as the radius was applied to obtain the final input domain. Figure 15 shows an example of the relationships between maximal nodal displacement and normalized angel and radius for both FE simulation (marked as stars) and metamodel (represented by surface).

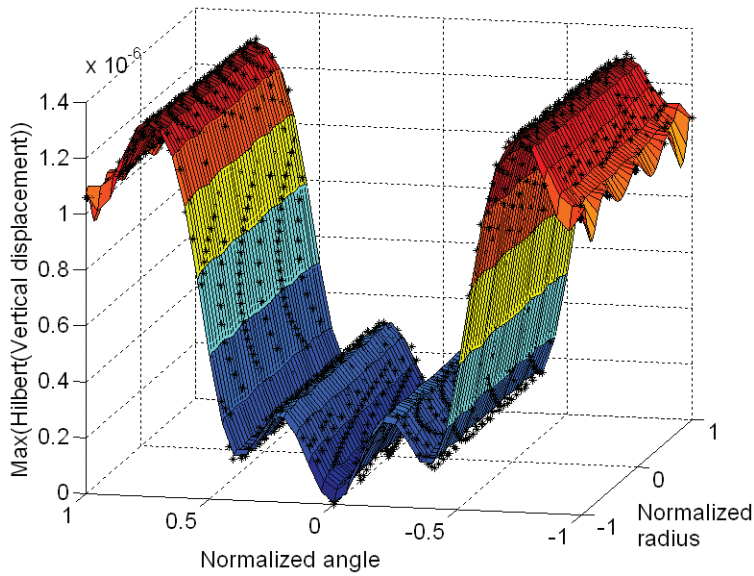

Figure 15. Approximated maximal nodal displacements

The metamodels for all 20 checked design configurations characterize high quality. The minimum value found for both the coefficient of multiple determination and adjusted coefficient of multiple determination equals 0.9974 [29,31].

In the last step of a single FE analysis the angle for the main lobe of beampattern was determined on the basis of approximated maximal nodal displacement. Having elaborated metamodels the maximal nodal displacements were found for the exact value of the radius, i.e. 150mm for which the normalized value equals 0, and uniformly distributed angles i.e. the normalized value varied from -1 up to 1 with a constant step. An example of the plot of beampattern found for the maximal nodal displacements presented in polar coordinate system is shown in Figure 16.

The angle of main lobe of beampattern was determined according to the criterion of -6dB reduction of the nodal displacement [32], i.e. current direction is considered to be within the angle of the main lobe of beampattern if related value of nodal displacement is not less than of -6dB decrease with respect the maximal value found for the whole beampattern. The results obtained for each checked configuration, i.e. amplitudes A_0, S_0, A'_0, S'_0 and the angle α, were used for the sensitivity analysis and design optimization procedure which are discussed in section 5 and 6 respectively.

5. SENSITIVITY ANALYSIS

The process of design optimization was preceded by the sensitivity analysis. In the analysis 2 geometry properties of apodized electrodes pattern of IDT were assumed as input parameters, i.e. the finger width W and length L. As the output parameters the following

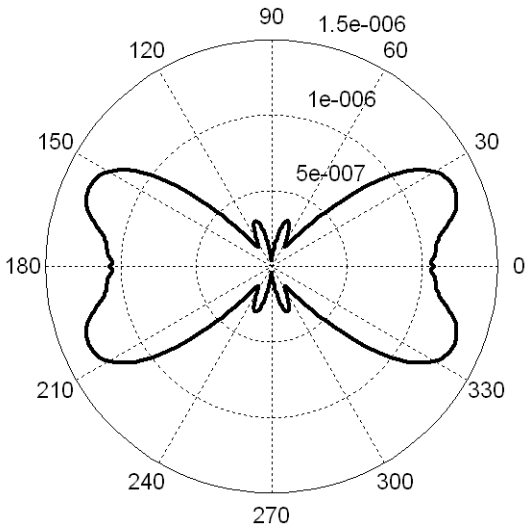

Figure 16. Beampattern for IDT

quantities were chosen to be important for the performance of designed IDT:

- the angle of main lobe of beampattern: α
- the amplitude of the A0 mode measured for desired direction of propagation: A_0
- the ratio for both the A0 and S0 modes measured for desired direction of propagation: $\frac{A_0}{S_0}$
- the ratio between amplitude of expected mode A0 and the sum of amplitudes of both A0 and S0 modes measured for undesired direction of propagation: $\frac{A_0}{A'_0 + S'_0}$

Listed above parameters seem crucial for the properties of IDT since it is expected to minimize the angle α for better wave directivity as well as maximize the amplitude of desired wave A0 in the horizontal direction. Moreover the ratios $\frac{A_0}{S_0}$ and $\frac{A_0}{A'_0 + S'_0}$ should be as high as possible to prevent from undesired contribution of the S0 mode in the main direction of wave propagation as well as both the A0 and S0 modes for perpendicular direction. All presented above priorities for the IDT improvement are included in the objective function of the optimization task which is discussed in the following section. Figure 17 presents normalized sensitivities S calculated for all considered criteria.

The normalized sensitivities $S = S_{i,j}$ were calculated accordingly to the formula:

$$S_{i,j} = \frac{\delta_{i,j}}{\delta_j} \cdot 100[\%] \tag{8}$$

where: $\delta_{i,j}$ is the maximal relative change of i-th output parameter while varying j-th input parameter, δ_j is the relative change of j-th input parameter, i stands for the index of output parameter, i.e. α for $i = 1$, A_0 for $i = 2$, etc, j denotes either the finger width (j=1) or the finger length (j=2). δ_j were found accordingly to the ranges of variation defined in the previous section.

The sensitivity analysis was performed for the quantitative assessment of the influence of input geometry characteristics on defined output parameters.

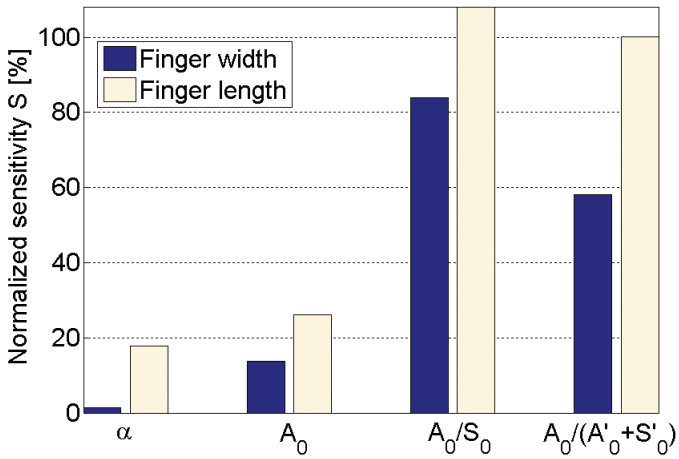

Figure 17. Normalized sensitivities

For assumed ranges of variation for input parameters the finger length L is more influential to all output criteria. For the ratio $\frac{A_0}{S_0}$ calculated normalized sensitivity even exceeds 100%. As far as the angle α is of concern, the influence of allowed variation of the finger width seems negligible. The finger length in apodized electrodes pattern in turn plays significant role for the wave directivity. Moreover the amplitude based criteria were found as much more sensitive than the angle of main lobe of beampattern.

Found sensitivities confirm that none of proposed criteria and input design parameters may be skipped in the objective function for the optimization task, i.e. for both the finger width and length there exist criteria with significant sensitivities as well as for each output criterion there exist at least one considerably influential input parameter.

6. DESING OPTIMIZATION

In present study the multi-criteria optimization task was performed to find the best configuration of 2 design parameters, i.e. the width W and length L of the outer fingers for linearly apodized IDT, in terms of both the angle of main lobe of beampattern α and other chosen amplitude based criteria. All the considered criteria were described in details in the context of sensitivity analysis. Minimized objective function takes the following form:

$$F(\mathbf{X}) = w\alpha - (1-w)\left(A_0 + \frac{A_0}{S_0} + \frac{A_0}{A'_0 + S'_0}\right) \tag{9}$$

where $w(0 \le w \le 1)$ denotes the weighting function which determines the priority for the optimization, i.e. either minimization of the angle α to better the directivity of generated waves or maximization of the contribution of A0 mode for the main direction with respect to the S0 mode for the same direction as well as for both the A0 and S0 modes for undesired perpendicular direction of propagation. The vector $\mathbf{X}$ determines the design configuration: the finger width W and length L. Allowed ranges of their variation equals:

- for the finger width : [0.7mm, 1.9mm]
- for the finger length : [3mm, 12mm]

To create 4 surfaces that represent the continuous relationships between decision variables, i.e. design variables W and length L, and criteria of the optimization, i.e. α, A_0, $\frac{A_0}{S_0}$ and $\frac{A_0}{A'_0 + S'_0}$, the RSM was applied for the results of 20 already checked design configurations which are described in section 4. All the output criteria were normalized to vary within the range [0,1] and then the metamodel fitting procedure was applied 4 times to determine all the approximations. Applied metamodels consider 16 regressors of up to the 3rd order. Examples of the plots of the objective functions calculated for $w = 0.5$ with both FE analyses and metamodels are shown in Figure 18 and 19 respectively.

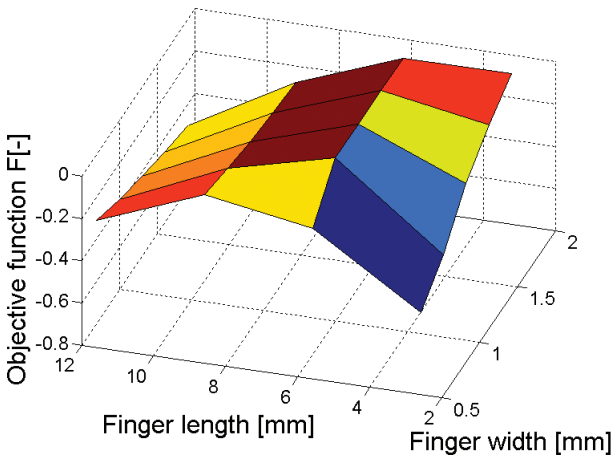

Figure 18. Objective function for w=0.5 calculated with FE analyses

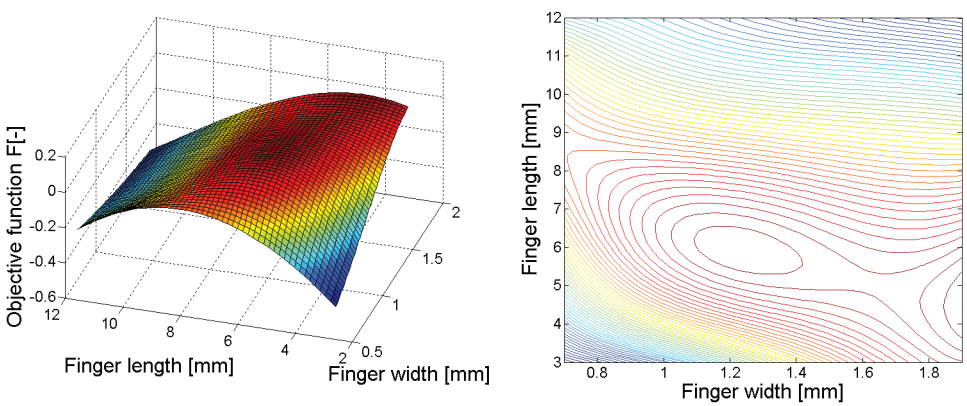

Figure 19. Objective function with contour plot for w=0.5 calculated with RSM

All determined metamodels are of high quality. The minimum value of the coefficient of multiple determination and adjusted coefficient of multiple determination found for all metamodels respectively equal 0.996 and 0.995.

The objective function found with RSM was used for the optimization with gradually increased values of weighting function w, with the step of 0.01. GA were applied to search for the best design configuration [33,34]. Applied GA characterize the following arbitrary assumed properties: number of individuals – 100, number of generations – 50, generation gap – 0.8, probability of crossover – 0.7, probability of mutation – 0.4. An example of the path for the best fitted individuals is presented in Figure 20.

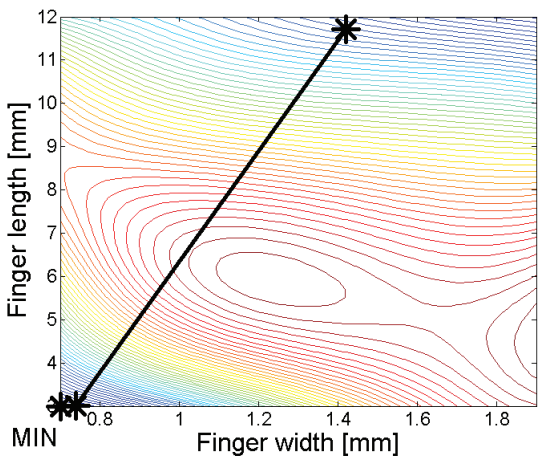

Figure 20. Example of the path for best fitted individuals for $w = 0.5$

The optimization task performed for subsequent values of the weighting function resulted in 2 optimal designs as presented in Figure 21. The Pareto plot is shown in Figure 22 in which both the minimized angle of main lobe α and the maximized sum of the amplitude based criteria $A_0 + \frac{A_0}{S_0} + \frac{A_0}{A'_0 + S'_0}$ are of concern.

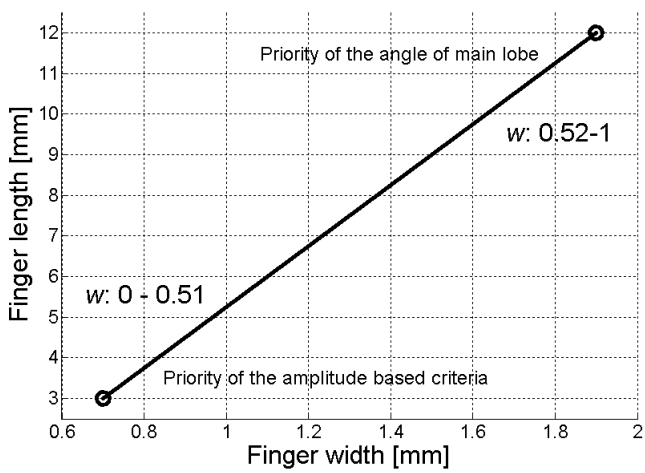

Figure 21. Optimal designs of apodized IDT

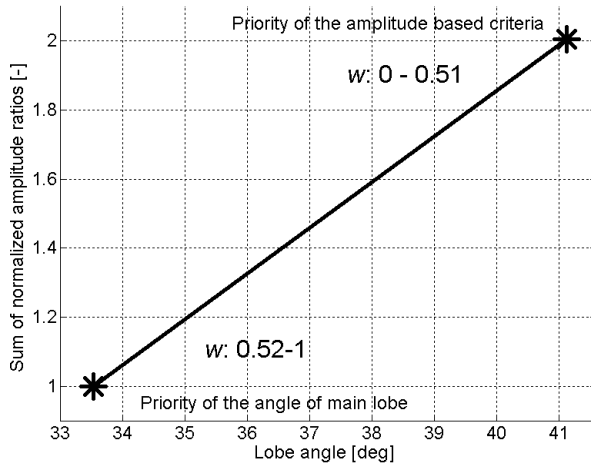

Figure 22. Optimal values of the criteria – Pareto frontier

Depending on given priority the following design configuration can be found:

- for $w \in [0,0.51]$ (priority of the amplitude based criteria): the finger width W=0.7mm, the finger length L=3mm, the angle α=41.1deg, the sum of amplitude based criteria equals 2.01
- for $w \in$ (priority of the angle of main lobe): the finger width W=1.9mm, the finger length L=12mm, the angle α=33.5deg, the sum of amplitude based criteria equals 1.00

In case when the amplitude based criteria are of higher importance the outer fingers of apodized electrode pattern should characterize possible smallest width and length simultaneously. For the case when the wave directivity is the most important the outer fingers should be as long and wide as possible in turn.

7. SUMMARY AND CONCLUDING REMARKS

The paper presents the results of sensitivity analysis and design optimization performed for the model of apodized IDT. The FE model of an aluminium plate with mounted piezoelectric transducer was parameterized to allow for a search of the best design configuration in terms of transducer performance. The width and length of the outer fingers were assumed as design parameters, therefore the optimization task was performed to search for the best electrode pattern that satisfy the compromise between competitive criteria on the angle of main lobe and the amplitudes of selected Lamb wave modes. The amplitude criteria considered increase of the amplitude of antisymmetric mode A0 for the main direction and the reduction of the amplitude of undesirable symmetric mode S0 for the same direction, as well as the amplitude reduction for both the A0 and S0 modes for undesired perpendicular direction of propagation. Mentioned criteria were chosen in order to obtain the best directivity and mode selectivity of the generated beampattern.

The introduction of weighting factor allowed to successfully control the balance between contributions of mentioned above criteria. The application of both RSM and GA enabled for effective search through the input domain of feasible design configurations of modelled IDT and finally there were proposed two different designs characterizing either good wave directivity or increased amplitude ratios.

ACKNOWLEDGEMENTS

The work was supported by the Polish Grant no. N N503 159240, which deals with the *Technology of the ultrasonic micro-transducers in Lamb waves based SHM*.

REFERENCES

1. Staszewski W.J., Ultrasonic/Guided Waves for Structural Health Monitoring, *Key Engineering Materials*, 2005, 293-294, 49-62.
2. Rose J.L., A vision of ultrasonic guided wave inspection potential, *Proceedings of the Seventh ASME NDE Topical Conference NDE*, 2001, Vol. 20.
3. Achenbach J.D., *Wave Propagation in Elastic Solids*, North-Holland Publishing Company, Amsterdam, 1973.
4. Lee B.C., Staszewski W.J., Lamb wave propagation modelling for damage detection: II. Damage monitoring strategy, *Smart Mater. Struct.*, 2007, 16, 260–274.
5. Ambrozinski L., Stepinski T., Packo P., Uhl T., Self-focusing Lamb waves based on the decomposition of the time-reversal operator using time–frequency representation, *Mechanical Systems and Signal Processing*, 2012, 27, 337–349.
6. Inman D.J., Farrar C.R., Lopes V. Jr., Steffen V. Jr. [ed.]: *Damage prognosis. For aerospace, civil and mechanical systems*, John Willey & Sons, Ltd., Chichester, England, 2005.
7. Alleyne D.N., Cawley P., The interaction of Lamb waves with defects. *IEEE Transactions on Ultrasonics, Ferroelectrics and Frequency Control*, 1992, 39(3), 381-397.
8. Degertekin F.L., Khuri-Yakub B.T., Lamb wave excitation by Hertzian contacts with application, *NDEIEEE Transactions on Ultrasonics, Ferroelectrics, and Frequency Control*, 1997, 44, 769-779.
9. Dutton B., Boonsang S., Dewhurst R.J., A new magnetic configuration for a small in-plane electromagnetic acoustic transducer applied to laser ultrasound measurements: Modelling and validation, *Sensors and Actuators A: Physical*, 2006, 125, 249-259.
10. Mirkhani K., Chaggares C., Masterson C., Jastrzebski M., Dusatko T., Sinclair A., Shapoorabadi R.J., Konrad A., Papini M., Optimal design of EMAT transmitters, *NDT&E International*, 2004, 37(3), 181-193.
11. Silva M.Z., Gouyon R., Lepoutre F., Hidden corrosion detection in aircraft aluminium structures using laser ultrasonics and wavelet transform signal analysis, *Ultrasonics*, 2003, 41, 301-305.
12. Ergun A.S., Yaralioglu G.G., Khuri-Yakub B.T.: Capacitive Micromachined Ultrasonic Transducers: Theory and Technology, *Journal of Aerospace Engineering*, 2003, 76-84.
13. Ergun A.S., Huang Y., Zhuang X., Oralkan O., Yaralioglu G.G, Khuri-Yakub B.T., Capacitive Micromachined Ultrasonic Transducers: Fabrication Technology, *IEEE Transactions on Ultrasonics, Ferroelectrics and Frequency Control*, 2005, 12, 2242-2258.
14. Martowicz A., Rosiek M., Manka M., Uhl T., Improving the design of capacitive micromachined ultrasonic transducers aided with sensitivity analysis, *International Journal of Multiphysics*, 2011, 5(2), 157-172.
15. Meynier C., Teston F., Certona D., A multiscale model for array of capacitive micromachined ultrasonic transducers, *Journal of the Acoustical Society of America*, 2010, 128 (5), 2549–2561.
16. Wong S.H., Kupnik M., Zhuang X., Lin D.-S., Butts-Pauly K., Khuri-Yakub B., Evaluation of wafer bonded CMUTs with rectangular membranes featuring high fill factor, *IEEE Transactions on Ultrasonics, Ferroelectrics, and Frequency Control*, 2008, 55(9), 2053-2065.
17. Badcock R.A., Birt E.A., The use of 0–3 piezocomposite embedded Lamb wave sensors for detection of damage in advanced fibre composites, *Smart Materials and Structures*, 2000, 291-297.
18. Schulz M.J., Pai P.F., Imman D.J., Health monitoring and active control of composite structures using piezoceramic patches, *Composites, Part B*, 1999, 30, 713-725.
19. Raghavan A., Cesnik C.E.S., Review of Guided-wave Structural Health Monitoring. *The shock and vibration digest*, 2007, 39(2), 91-114.
20. Williams B.R., Park G., Inman D.J., Wilkie K.W., An Overview of Composite Actuators with Piezoceramic Fibers, *Proceedings of the 20th International Modal Analysis Conference*, Los Angeles, 2002, 421-427.

21. Sodano H.A., Park G., Inman D.J., An investigation into the performance of macro-fiber composites for sensing and structural vibration applications, *Mechanical Systems and Signal Processing*, 2004, 18, 683-697.
22. Na J.K., Blackshire J.L., Kuhra S., Design, fabrication and characterization of single-element interdigital transducers for NDT applications, *Sensors and Actuators A*, 2008, 148, 359-365.
23. Manka M., Rosiek M., Martowicz A., Uhl T., Interdigital transducers for Lamb-wave based SHM systems: design and sensitivity analysis. *Mechanics And Control*, 2011, 30(2).
24. Manka M., Rosiek M., Martowicz A., Uhl T., Stepinski T., Properties of interdigital transducers for lamb-wave based SHM systems, Chang F.-K. [ed.], *Structural health monitoring 2011, Condition-based maintenance and intelligent structures, Proceedings of the 8th international workshop on Structural Health Monitoring*, Stanford, September 13–15, 2011, Vol. 2, 1488–1495.
25. Mamishev A.V., Sundara-Rajan K., Yang F., Du Y., Zahn M., Interdigital Sensors and Transducers, *Proceedings of the IEEE*, 2004, 92(5).
26. Castaings M., Monkhouse R.S.C., Lowe M.J.S., Cawley P., The Performance of Flexible Interdigital PVDF Lamb Wave Transducers, *Acustica and Acta Acustica*, 1999, 85, 842- 849.
27. *ANSYS Modeling and Meshing Guide*, ANSYS Inc., Canonsburg, 2007.
28. http://www.smart-material.com/
29. Box G.E.P., Draper N.R., *Empirical Model Building and Response Surfaces*, John Wiley & Sons, Inc., New York, 1986.
30. Martowicz A., Klepka A., Uhl T., Application of Response Surface Method to model static and dynamic properties of MEMS structure, *Proceedings of Multiphysics 2009*, Lille, France, December 9-11, 2009.
31. Myers R.H., Montgomery D.C., *Response Surface Methodology process and product optimization using designed experiments*, John Wiley & Sons, Inc., New York, 1995.
32. *Ultrasonic Transducers Technical Notes OLYMPUS NDT*, http://www.olympusNDT.com, 2006.
33. Goldberg D.E., *Genetic algorithms in search, optimization, and machine learning*, Addison-Wesley Publishing Company, Reading, Massachusetts, U.S.A., 1989.
34. Michalewicz Z., *Genetic algorithms + data structures = evolution programs*, Springer-Verlag, Berlin, Heidelberg 1996.